

# A conclusive non-detection of magnetic field in the Am star $\alpha$ Peg with high-precision near-infrared spectroscopy<sup>★</sup>

O. Kochukhov<sup>1</sup>, A. M. Amarsi<sup>1</sup>, A. Lavail<sup>2</sup>, H. L. Ruh<sup>3</sup>, A. Hahlin<sup>1</sup>, A. Hatzes<sup>4</sup>, E. Nagel<sup>3</sup>, N. Piskunov<sup>1</sup>, K. Pouilly<sup>5</sup>,  
A. Reiners<sup>3</sup>, M. Rengel<sup>6</sup>, U. Seemann<sup>7,3</sup>, and D. Shulyak<sup>8</sup>

<sup>1</sup> Department of Physics and Astronomy, Uppsala University, Box 516, S-75120 Uppsala, Sweden  
e-mail: oleg.kochukhov@physics.uu.se

<sup>2</sup> Institut de Recherche en Astrophysique et Planétologie, Université de Toulouse, CNRS, IRAP/UMR 5277, 14 avenue Edouard Belin, F-31400, Toulouse, France

<sup>3</sup> Institut für Astrophysik und Geophysik, Georg-August-Universität, Friedrich-Hund-Platz 1, 37077 Göttingen, Germany

<sup>4</sup> Thüringer Landessternwarte Tautenburg, Sternwarte 5, 07778 Tautenburg, Germany

<sup>5</sup> Department of Astronomy, University of Geneva, Chemin Pegasi 51, CH-1290 Versoix, Switzerland

<sup>6</sup> Max-Planck-Institut für Sonnensystemforschung, Justus-von-Liebig-Weg 3, 37077 Göttingen, Germany

<sup>7</sup> European Southern Observatory, Karl-Schwarzschild-Str. 2, 85748 Garching bei München, Germany

<sup>8</sup> Instituto de Astrofísica de Andalucía – CSIC, Glorieta de la Astronomía s/n, 18008 Granada, Spain

Received 29 April 2024 / Accepted 21 May 2024

## ABSTRACT

**Context.** The A-type metallic-line (Am) stars are typically considered to be non-magnetic or possessing very weak sub-G magnetic fields. This view has been repeatedly challenged in the literature, most commonly for the bright hot Am star  $\alpha$  Peg. Several studies claimed to detect 1–2 kG field of unknown topology in this object, possibly indicating a new process of magnetic field generation in intermediate-mass stars.

**Aims.** In this study, we revisit the evidence of a strong magnetic field in  $\alpha$  Peg using new high-resolution spectropolarimetric observations and advanced spectral fitting techniques.

**Methods.** The mean magnetic field strength in  $\alpha$  Peg is estimated from the high-precision CRIRES<sup>+</sup> measurement of near-infrared sulphur lines. This observation is modelled with a polarised radiative transfer code, including treatment of the departures from local thermodynamic equilibrium. In addition, the least-squares deconvolution multi-line technique is employed to derive longitudinal field measurements from archival optical spectropolarimetric observations of this star.

**Results.** Our analysis of the near-infrared Si I lines reveals no evidence of Zeeman broadening, ruling out magnetic field with a strength exceeding 260 G. This null result is compatible with the relative intensification of Fe II lines in the optical spectrum taking into account blending and uncertain atomic parameters of the relevant diagnostic transitions. Longitudinal field measurements at three different nights also yield null results with a precision of 2 G.

**Conclusions.** This study refutes the claims of kG-strength dipolar or tangled magnetic field in  $\alpha$  Peg. This star is effectively non-magnetic, with the surface magnetic field characteristics no different from those of other Am stars.

**Key words.** stars: chemically peculiar – stars: early-type – stars: magnetic field – stars: individual:  $\alpha$  Peg

## 1. Introduction

The upper main sequence stars, with spectral classes from early B to early F, can be separated into two distinct groups according to their surface magnetic field characteristics (Preston 1974; Donati & Landstreet 2009). One group, the so-called magnetic chemically peculiar (mCP) or Ap/Bp stars, exhibits stable, globally-organised kG-strength fields on stellar surfaces. These objects comprise about 10% of all intermediate-mass and massive stars (Grunhut et al. 2017; Schöller et al. 2017; Sikora et al. 2019). Another, more sizeable, group includes normal and non-magnetic chemically peculiar stars, which show no evidence of strong organised surface magnetic fields. The cool end of the temperature sequence of non-magnetic CP stars is populated by the metallic-line A-type (Am) stars. These stars are known for their slow rotation, common membership in close binary sys-

tems, a moderate overabundance of iron-peak elements, and an underabundance of Ca and Sc (e.g. Ghazaryan et al. 2018). The brightest star in the sky, Sirius, is an example of a hot Am star (Landstreet 2011; Cowley et al. 2016).

The spectroscopic characteristics of Am stars facilitate precise measurements of the mean longitudinal magnetic field,  $\langle B_z \rangle$ , using high-resolution circular polarisation observations (Wade et al. 2000). Applications of this technique, only sensitive to a global magnetic field component, ruled out the presence of  $\geq 10$  G large-scale fields in Am stars (Shorlin et al. 2002; Aurière et al. 2010). This upper limit is at least one order of magnitude below the  $\sim 100$  G weak-field limit of mCP stars (Aurière et al. 2007; Kochukhov et al. 2023a). The observational picture of Am-star magnetism becomes more nuanced for weaker fields. Definitive  $\langle B_z \rangle$  measurements at a level of 5–10 G, compatible with a global dipolar-like field sheared by a differential rotation, were reported for at least one Am star,  $\gamma$  Gem (Blazère et al. 2020). At the same time, circular polarisation signatures corresponding to sub-G magnetic fields were detected in several

<sup>★</sup> Based on guaranteed time observations (GTO) collected at the European Southern Observatory (ESO) under ESO programs 0111.D-0297 by the CRIRES<sup>+</sup> consortium.

bright Am stars (Petit et al. 2011; Blazère et al. 2016; Neiner et al. 2017). Considering a conspicuous gap in the magnetic field strength distribution between Am and mCP stars, and different geometrical characteristics of their fields, the ultra-weak Am star magnetism likely has a different physical origin compared to stable fossil fields found in mCP stars (Cantiello & Braithwaite 2019; Jermyn & Cantiello 2020).

The view that Am stars are either non-magnetic or host only very weak fields is occasionally challenged in the literature. The star *o* Peg (43 Peg, HR 8641, HD 214994) is in the centre of this debate. This is a bright, narrow-line hot Am star, frequently targeted by detailed chemical abundance and model atmosphere analyses based on high-resolution optical (Adelman 1988; Landstreet et al. 2009; Takeda et al. 2012; Adelman et al. 2015) and ultra-violet (Adelman et al. 1993) spectra. No longitudinal magnetic field was detected in this star by Shorlin et al. (2002). Their single magnetic field measurement,  $\langle B_z \rangle = -32 \pm 20$  G, is compatible with zero, albeit at the precision inferior relative to what has been achieved for similarly bright stars in more recent studies. On the other hand, Mathys & Lanz (1990) reported the presence of  $\approx 2$  kG mean magnetic field,  $\langle B \rangle$ , in *o* Peg from a statistical line-width analysis and an empirical relation between  $\langle B \rangle$  and relative equivalent widths of the Fe II 614.7 and 614.9 nm lines. Takeda (1991) studied the behaviour of this line pair in a magnetic field using radiative transfer calculations, confirming  $\sim 2$ – $3$  kG magnetic field in *o* Peg. Subsequently, Takeda (1993) measured  $\sim 2$  kG field by minimising the scatter of abundances derived from lines of different strength. These results were recently revised by Takeda (2023), who analysed new high-quality spectroscopic observations of *o* Peg with several of the aforementioned techniques and concluded, once again, that *o* Peg possesses  $\langle B \rangle \approx 1$ – $2$  kG.

The vast discrepancy between  $\sim$  kG field strength inferred from the Stokes *I* spectra and  $\sim 50$  G upper limit obtained from Stokes *V* observations is usually interpreted assuming that the putative field of *o* Peg is “complex” or “tangled”, meaning that it is dominated by a small-scale component that produces broadening and intensification of line profiles in the Stokes *I* spectra but remains undetectable in Stokes *V* due to cancellation of the contributions of the surface regions with different field polarities to the disk-integrated stellar polarisation spectra. This situation is often found in cool active stars with dynamo fields (e.g. Kochukhov et al. 2020, 2023b; Kochukhov 2021), although the ratio  $\langle B \rangle / \langle B_z \rangle \sim 100$  implied by the previous magnetic field studies *o* Peg appears to be exceptionally large even compared to cool stars. Contrary to this picture, Takeda (2023) postulated that *o* Peg has a global dipolar magnetic field viewed from the magnetic equator, implying that the null  $\langle B_z \rangle$  measurement by Shorlin et al. (2002) is explained by a fortuitous cancellation of the signals from the positive and negative magnetic hemispheres.

This series of seemingly consistent magnetic field determinations for *o* Peg is having a noticeable influence on the community’s understanding of Am stars in general. The work by Mathys & Lanz (1990) is frequently brought up in review papers (Landstreet 1992; Dworetzky 1993; Smith 1996; Kurtz & Martinez 2000; Mathys 2004a,b, 2009; Hubrig & Schöller 2021). It inspired applications of the same magnetic field measurement procedures to other Am stars (Lanz & Mathys 1993; Savanov 1994; Scholz et al. 1997), to their hotter counterparts, HgMn stars (Takada-Hidai & Jugaku 1992; Hubrig & Castelli 2001; Kochukhov et al. 2013), and to other A-type stars (Takada-Hidai & Jugaku 1993). In a wider context, some authors consider the presumed complex and strong magnetic field of *o* Peg to be representative of all Am stars (e.g. Drake et al. 1994). However,

the majority of studies adopt a more conservative viewpoint that this star is, for some reason, exceptional in terms of its magnetic characteristics (Debernardi et al. 2000; Hui-Bon-Hoa 2000; Carrier et al. 2002; Korčáková et al. 2022).

In the present study, we revisit the question of whether or not *o* Peg is a magnetic star. To this end, we use new spectropolarimetric measurements to characterise the global magnetic field component at a far greater precision than in previous studies. Moreover, we investigate the Zeeman effect using high signal-to-noise (S/N) optical and, for the first time for any Am star, near-infrared high-resolution spectra. The paper is structured as follows. We start with an overview of the observational data employed in this study (Sect. 2). We proceed to describe our polarised spectrum synthesis methodology in Sect. 3, including assessment of the deviations from the local thermodynamic equilibrium and partial Paschen-Back (PPB) splitting. This is followed by the analysis of near-infrared (Sect. 4) and optical (Sect. 5) profiles of magnetically sensitive lines, leading to a new sensitive upper limit on the total magnetic field strength of *o* Peg. We complement this analysis with high-precision spectropolarimetric measurements of the longitudinal field (Sect. 6) and derivation of an upper limit of the dipolar magnetic component compatible with these observations. The paper is concluded with the summary and discussion in Sect. 7.

## 2. Observations

### 2.1. Near-infrared spectroscopy

We observed *o* Peg on August 12 2023 with the upgraded CRYogenic InfraRed Echelle Spectrograph (CRIRES<sup>+</sup>, Dorn et al. 2023) at the European Southern Observatory (ESO) Very Large Telescope (VLT) located on Cerro Paranal, Chile. CRIRES<sup>+</sup> is a high-resolution ( $R \approx 10^5$ ) cross-dispersed near-infrared spectropolarimeter mounted on a Nasmyth focus of the 8-m Unit Telescope 3 at the VLT. Our observations were carried out as part of the CRIRES<sup>+</sup> consortium Guaranteed Time Observations.

The instrument was setup with a slit width of 0.2 arcsecond, and we obtained observations in four standard wavelength settings: Y1029, J1228, H1567, and H1582. For observations carried in each wavelength setting, we obtained 8 individual exposures with a 30-s integration time, taken with an AAAABBBB nodding pattern. The nodding procedure consists in placing the star on two distinct positions (A and B) on the slit and facilitates the removal of sky background and detector artefacts in the data reduction. The log of our CRIRES<sup>+</sup> observations of *o* Peg is presented in Table 1.

To reduce the data, we used the CRIRES<sup>+</sup> data reduction pipeline `cr2res` (Dorn et al. 2023). First, we reduced the raw calibration frames association with our programme taken as part of the daily calibration routine. These data consist of darks, flat fields, and wavelength calibration frames (Fabry-Perot etalon, Uranium-Neon lamp) and were reduced using the standard calibration reduction cascade as laid out in the `cr2res` pipeline user manual<sup>1</sup>.

We then reduced the science data for each wavelength setting using the `cr2res_obs_nodding` recipe. It applies the reduced calibrations to the science raw frames (bad pixel mask, pixel-to-pixel sensitivity), subtracts the B frames from the A frames, extracts the 1D science and error spectra for the two nodding positions using an optimal extraction algorithm, and applies the wavelength solution to the spectra.

<sup>1</sup> <https://www.eso.org/sci/software/pipelines/cr2res/cr2res-pipe-recipes.html>

**Table 1.** Log of CRIRES<sup>+</sup> observations of *o* Peg.

UTC date	UTC time at start	Wavelength setting	Integration time	Median S/N per pixel
2023-08-12	05:25:09.087	Y1029	8x30 seconds	372
2023-08-12	05:33:12.845	J1228	8x30 seconds	379
2023-08-12	05:42:15.479	H1567	8x30 seconds	335
2023-08-12	05:51:06.603	H1582	8x30 seconds	309

**Table 2.** Mean longitudinal magnetic field measurements derived from the ESPaDOnS observations.

UT date	HJD	S/N	S/N <sub>LSD</sub>	$\langle B_z \rangle$ (G)
10-06-2014	2456819.122	946	41391	$-2.3 \pm 2.1$
15-06-2014	2456824.094	938	40650	$-3.1 \pm 2.2$
19-06-2014	2456828.069	972	41964	$1.5 \pm 2.1$

**Notes.** Columns give the UT date and heliocentric Julian date of mid-exposure, the S/N per pixel in the extracted spectrum at 520 nm, the average S/N of the LSD Stokes *V* profile, and the resulting measurement of the mean longitudinal magnetic field.

The analysis presented below (Sect. 4) focuses on the S I lines at 1046 nm observed in the Y1029 setting. The S/N reached at this wavelength is around 480 according to the formal error propagation by the *cr2res* pipeline. This agrees with the empirical measurement of the standard deviation of continuum points in the vicinity of the S I lines.

## 2.2. Optical spectroscopy

Considering particular importance and common historic as well as current usage of the Fe II 614.7–614.9 nm line pair for measuring magnetic fields in chemically peculiar stars, including *o* Peg, we revisit this magnetic diagnostic in Sect. 5. At the same time, we refrain from re-assessing all types of magnetic detection methods applied to *o* Peg and similar stars based on Stokes *I* profiles of optical lines since the near-infrared magnetic diagnostic technique developed in our paper (Sect. 4) is by far superior in terms of its ability to detect magnetic fields.

Among multiple optical archival spectra of *o* Peg covering this line pair, we chose to use the observed spectrum published by Takeda (2023) due to its higher resolution and better S/N. This spectrum was constructed from a series of individual observations obtained over several nights in October 2008 using the HIDES coude echelle spectrograph at the 1.88 m telescope of Okayama Astrophysical Observatory. The spectrum has a resolving power of  $\lambda/\Delta\lambda \approx 10^5$  and a very high S/N approaching 1000. Further details on the acquisition and reduction of these data can be found in Takeda et al. (2012) and Takeda (2023).

## 2.3. Optical spectropolarimetry

Three previously unpublished circular polarisation observations of *o* Peg are included in the PolarBase archive (Petit et al. 2014). These spectra were obtained on three non-consecutive nights between June 10 and June 19, 2014 with the ESPaDOnS spectropolarimeter (Donati et al. 2006) installed at the 3.6 m Canada-France-Hawaii telescope. For each observation, the intensity (Stokes *I*) and circular polarisation (Stokes *V*) spectra were recorded using a sequence of four 110-s sub-exposures, resulting in a peak S/N of 940–970 per pixel of the extracted intensity spectrum at  $\lambda = 520$  nm. The individual times of mid-exposure and S/N values are provided in Table 2.

The ESPaDOnS spectra have a fixed format that covers the 370–1030 nm wavelength range with 40 partially overlapping echelle orders at a resolving power of  $\lambda/\Delta\lambda = 65000$ . The *o* Peg observations were reduced by the Libre-ESpRIT pipeline (Donati et al. 1997) running at the telescope. We post-processed the spectra, aiming to improve continuum normalisation, with the help of the procedures described in Rosén et al. (2018). In this study, the ESPaDOnS circular polarisation observations are employed to obtain new measurements of the mean longitudinal magnetic field and derive constraints on the global magnetic field geometry in Sect. 6.

## 3. Modelling methodology

### 3.1. Polarised spectrum synthesis

The spectrum synthesis modelling carried out in this paper is based upon the polarised radiative transfer code *Synmast* (Kochukhov 2007; Kochukhov et al. 2010). This software derives a numerical solution of the polarised radiative transfer equation for a given model atmosphere, limb angle, and local magnetic field vector. *Synmast* shares the equation of state module with the Spectroscopy Made Easy (SME) package (Piskunov & Valenti 2017) and has been extensively tested against independent polarised radiative transfer codes (Wade et al. 2001).

In the calculations for the present paper, we adopted a simplified model of stellar magnetic field comprised of a uniform radial field distribution. This approach, widely used in modelling Zeeman broadening and intensification effects in the Stokes *I* spectra of active stars (e.g. Lavail et al. 2019; Kochukhov et al. 2020; Hahlin et al. 2023), requires calculation of a small number (typically seven) of local intensity spectra at different limb angles to obtain accurate disk-integrated profiles. Since the radial field is seen from different aspect angles depending on the centre-to-limb position, its cumulative effect on the Zeeman split line profiles is more representative of possible complex magnetic configuration than any field geometry defined relative to the observer’s line of sight (e.g. a purely transverse or purely longitudinal field). In fact, the disk-integrated Stokes *I* line profiles corresponding to a uniform radial magnetic field turn out to be very similar to those calculated for a star covered by an anisotropic randomly oriented field with the same strength. Therefore, our model is compatible with the hypothesis of a complex tangled magnetic field entertained by some previous studies of *o* Peg.

The model atmosphere employed in the present study was calculated with the LLmodels code (Shulyak et al. 2004) assuming the effective temperature  $T_{\text{eff}} = 9500$  K, surface gravity  $\log g = 3.6$ , and microturbulent velocity  $\xi_t = 2$  km s<sup>-1</sup>. These are typical atmospheric parameter values inferred by modern detailed spectroscopic studies of *o* Peg (see the summary in Takeda 2023). For these model atmosphere calculations, we used individual chemical abundances of *o* Peg from Adelman et al. (2015).

It is not obvious which spectral lines are best suited for accurate magnetic field measurements in Stokes *I* in the available

**Table 3.** Atomic line data adopted for the S I NIR triplet.

Ion	$\lambda$ (nm) <sup>1</sup>	$\log gf^2$	$E_{lo}$ (eV)	Lower level		Upper level		$g_{eff}$	$\log \gamma_{rad}$	$\log \gamma_{stark}$	H broadening ( $\sigma_H/a_0^2, \alpha_H$ ) <sup>3</sup>
				$J_{lo}$	$g_{lo}$	$J_{up}$	$g_{up}$				
S I	1045.5451	0.250	6.8601	1.0	2.0	2.0	1.5	1.25	8.95	-5.37	625, 0.227
S I	1045.6757	-0.447	6.8601	1.0	2.0	0.0	0.0	2.00	8.95	-5.37	625, 0.227
S I	1045.9406	0.030	6.8601	1.0	2.0	1.0	1.5	1.75	8.95	-5.37	625, 0.227

**Notes.** (1) NIST, [Kramida et al. \(2022\)](#); (2) [Zerne et al. \(1997\)](#); (3) neutral hydrogen broadening cross-sections  $\sigma_H$  and exponents  $\alpha_H$  from [Barklem et al. \(2000\)](#); other parameters from VALD, [Ryabchikova et al. \(2015\)](#).

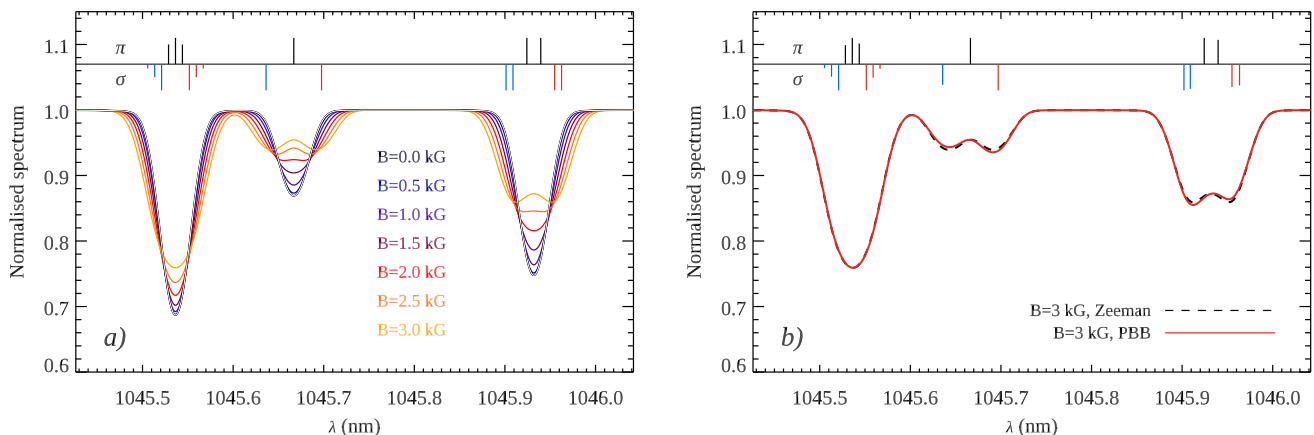


**Fig. 1.** **a)** Synthetic Zeeman profiles of the NIR S I triplet for different magnetic field strengths. The corresponding splitting patterns are shown schematically above each line for  $B = 3$  kG. **b)** Comparison of the Zeeman (black dashed line) and PPB (red solid line) calculations for  $B = 3$  kG. The splitting patterns above line profiles are illustrated for the PPB case.

wide wavelength coverage optical and NIR spectra of *o* Peg. In particular, spectral lines with the largest effective Landé factors are not necessarily the most informative diagnostics of weaker magnetic fields because subtle Zeeman broadening effects are often washed out by rotational broadening. As shown by several studies of cool active stars (e.g. [Kochukhov & Lavail 2017](#); [Kochukhov et al. 2020, 2023b](#)), spectral lines with above average effective Landé factors and complex Zeeman splitting patterns may provide useful alternative diagnostics owing to their strong magnetic intensification response. To identify the most suitable magnetically sensitive lines, we modelled the entire optical and NIR spectrum of *o* Peg with Synmast, comparing non-magnetic calculations with the theoretical spectra corresponding to  $B = 1$  and 2 kG. After applying the appropriate rotational and instrumental broadening, the S I triplet at 1045.5–1045.9 nm has emerged as the most promising diagnostic feature in the NIR wavelength region. The three components of this multiplet are well-separated for the projected equatorial velocity ( $v_e \sin i$ ) of *o* Peg and exhibit distinct magnetic responses due to different effective Landé factors (ranging from 1.25 to 2.00) and diverse Zeeman splitting patterns. The relevant line parameters of the S I triplet are summarised in Table 3, where we note that the absolute oscillator strengths of the three lines are measured with uncertainties of the order 0.01 dex ([Zerne et al. 1997](#)). There are no significant blending contributions to any of these three lines for the effective temperature and chemical abundance of *o* Peg.

Figure 1a illustrates a series of Synmast calculations of the S I triplet with increasing magnetic field strength. These spectra are convolved with the projected rotational velocity  $v_e \sin i = 5.9$  km s<sup>-1</sup>, macroturbulent velocity  $\zeta_t = 3.7$  km s<sup>-1</sup> (similar to the results obtained in Sect. 4), and a Gaussian instrumental profile corresponding to  $R = 10^5$  to represent instrumental broadening of our CRIRES<sup>+</sup> spectrum. The effect of magnetic

field becomes readily apparent already at  $B \approx 1$  kG, with the S I 1045.5 nm line exhibiting less excess magnetic broadening compared to the 1045.9 and, in particular, the 1045.7 nm line. The latter feature starts showing partially resolved Zeeman splitting at  $B \approx 2$  kG. This diverse magnetic response of lines of the same multiplet (or more generally of nearby lines of the same ion with similar excitation potentials and precise relative oscillator strengths) is ideal for disentangling magnetic broadening and intensification from competing broadening effects due to turbulent and rotational velocity fields. No other spectral lines with the diagnostic potential comparable to the S I triplet were found in our calculations for the CRIRES<sup>+</sup> wavelength region. Hence, we restricted the NIR part of our study to these S I lines. At the same time, we re-examined the Fe II 614.7–614.9 nm lines based on previously published observations (see Sect. 2.2) to address claims of magnetic field detections using this line pair.

### 3.2. Non-LTE effects

To fully utilise the diagnostic power of the S I 1046 nm triplet, departures from local thermodynamic equilibrium (LTE) must be taken into account. Previous studies of non-LTE effects for sulphur include theoretical investigations by [Takeda et al. \(2005\)](#) and [Korotin \(2009\)](#), and applications mainly to the Sun (e.g. [Scott et al. 2015](#)) and other FGK-type stars (e.g. [Nissen et al. 2007](#); [Caffau et al. 2016](#)), with fewer studies of warm stars (e.g. [Kamp et al. 2001](#)). All these studies point to significant effects for the neutral atom.

For this work we carried out our own non-LTE calculations for sulphur. The statistical equilibrium was solved for using Balder ([Amarsi et al. 2018b, 2022](#)). The departure coefficients generated by Balder were read into Synmast and used to correct the LTE line opacity and source function prior to spectrum

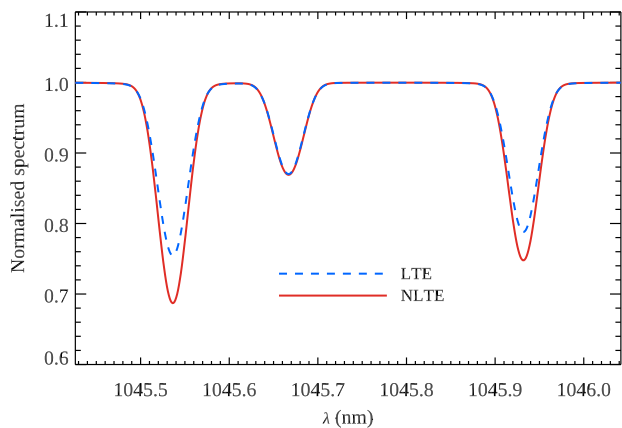


**Fig. 2.** Impact of departures from LTE on the synthetic profiles of the NIR S I triplet. These calculations were carried out for  $B = 0$  kG,  $\log N_S/N_{\text{tot}} = -4.35$ ,  $\xi_t = 2$  km s $^{-1}$  and other parameters of *o* Peg set to the best-fitting values found in Sect. 4.

synthesis, as described in Piskunov & Valenti (2017). Balder is based on Multi3D (Leenaarts & Carlsson 2009) but with several modifications, the most important for the present work relating to the equation of state and background opacities (calculated with Blue; Zhou et al. 2023). Rayleigh scattering in the UV was considered for hydrogen (Lee & Kim 2004) and helium (Langhoff et al. 1974), while other background transitions were treated in pure absorption.

The model atom was used in Carlos et al. (2024) and will also be described in a future paper (Amarsi et al., in prep.). In brief, the model atom contains 66 levels in total (including seven “super” levels of neutral sulphur, and four levels of ionised sulphur). Radiative transition data come from the National Institute of Standards and Technology (NIST, Kramida et al. 2022), based on the calculations of Zatsarinny & Bartschat (2006); and from the Opacity Project (e.g. Seaton et al. 1992). Electron collision data come from empirical recipes (van Regemorter 1962; Allen 1973). Hydrogen collisions were taken from Belyaev & Voronov (2020) and combined with data calculated using the recipe of Kaulakys (1991) in the scattering-length approximation (see Barklem 2016 and Amarsi et al. 2018a). Pressure broadening by electrons and by neutral hydrogen was taken into account based on data from the Kurucz database (e.g. Kurucz 1995) and by interpolating tables of hydrogen collisional cross-section data (Anstee & O’Mara 1995; Barklem & O’Mara 1997; Barklem et al. 1998).

The statistical equilibrium calculations were performed on the same LLmodels atmosphere used for the analysis described in Sect. 4. The microturbulent velocity  $\xi_t$  was fixed at 2.0 km s $^{-1}$ , which is close to the best-fitting result for *o* Peg (see Sect. 4). Assuming sulphur to be a trace element with no impact on the model atmosphere, the calculations were performed for a range of abundances  $\log N_S/N_{\text{tot}} = -4.60$  to  $-4.25$  ( $\log N_S/N_H + 12 = 7.42$  to 7.77), with step size of 0.05 dex.

The different components of the S I triplet are affected differently by departures from LTE, as seen in Fig. 2. At the best-fitting parameters of *o* Peg, the strength of the weakest, middle component is quite close to that in LTE, while the stronger blue and red components are significantly stronger in non-LTE. These effects can be understood from Fig. 3, which shows the departure coefficients of the lower and upper terms at the best-fitting abundance as a function of logarithmic Rosseland-mean optical depth  $\log \tau_{\text{Ross}}$ . To first order, the line opacity goes as the

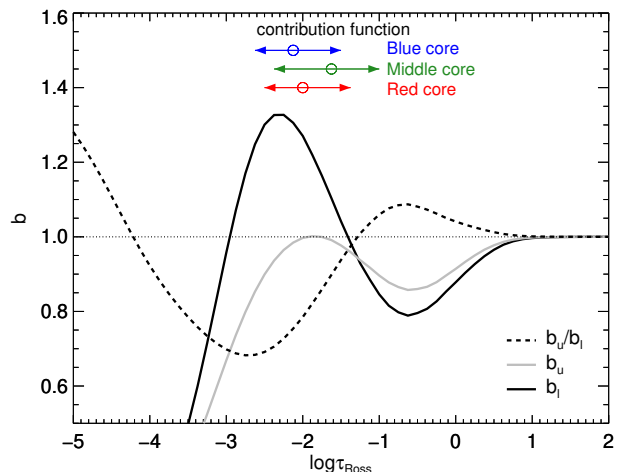


**Fig. 3.** Departure coefficients of the lower and upper levels of the S I triplet,  $b_l$  and  $b_u$  respectively. Their ratio is also shown. The full-width at half maximum (arrows) and peak depth (open circles) of the contribution functions to the depression in the disc-integrated flux, calculated at line-centre, are shown for the three lines of the S I triplet.

departure coefficient of the lower level  $b_l$ , while the line source function goes as the ratio of the upper and lower level departure coefficients  $b_u/b_l$  (e.g. Rutten 2003). The dip in  $b_l$  and  $b_u$  in deeper layers,  $\log \tau_{\text{Ross}} \approx -0.6$ , is caused by pumping due to absorption of UV photons in bound-free transitions (overionisation), resulting primarily in lower line opacity and a weakening of lines forming in this region. Towards higher layers, photon losses from high-lying transitions become significant. In particular, the S I triplet itself strongly regulates the populations of its levels such that  $b_l$  rises and  $b_u/b_l$  falls: they pass through unity at around  $\log \tau_{\text{Ross}} \approx -1.4$ .

The different effects on the three components are directly related to their different formation depths. This is because the model atom adopts efficient collisional coupling between the fine structure levels (e.g. Lind & Amarsi 2024), and so the departure coefficients are identical for the three components. The formation depths can be quantified via the contribution function to the depression in the disc-integrated flux (e.g. Albrow & Cottrell 1996; Amarsi 2015); these functions calculated at line-centre are overplotted in Fig. 3. The stronger blue and red components mostly form in layers  $\log \tau_{\text{Ross}} \lesssim -1.4$ , where  $b_l > 1$  and  $b_u/b_l < 1$ : the line opacity is increased relative to LTE and the line source function is reduced relative to LTE, and both act to increase the line strength. In contrast, the weakest middle component forms in deeper layers, where it suffers from both line strengthening and line weakening effects. Consequently, the broadened line profile appears closer to that predicted in LTE.

### 3.3. Partial Paschen-Back splitting

With the separation of the lower energy levels of  $\approx 4$  cm $^{-1}$ , the magnetic splitting of the Fe II 614.7–614.9 nm line pair studied in Sect. 5 is affected by the PPB effect (Mathys 1990). This phenomenon arises when the magnetic splitting of the atomic energy levels becomes comparable to the fine-structure splitting, resulting in asymmetric line splitting patterns. For lines forming in the PPB regime, both positions and strengths of the Zeeman components exhibit a complex non-linear behaviour with the magnetic field strength. However, deviation from the linear Zeeman splitting in the considered Fe II line pair are negligible for fields up

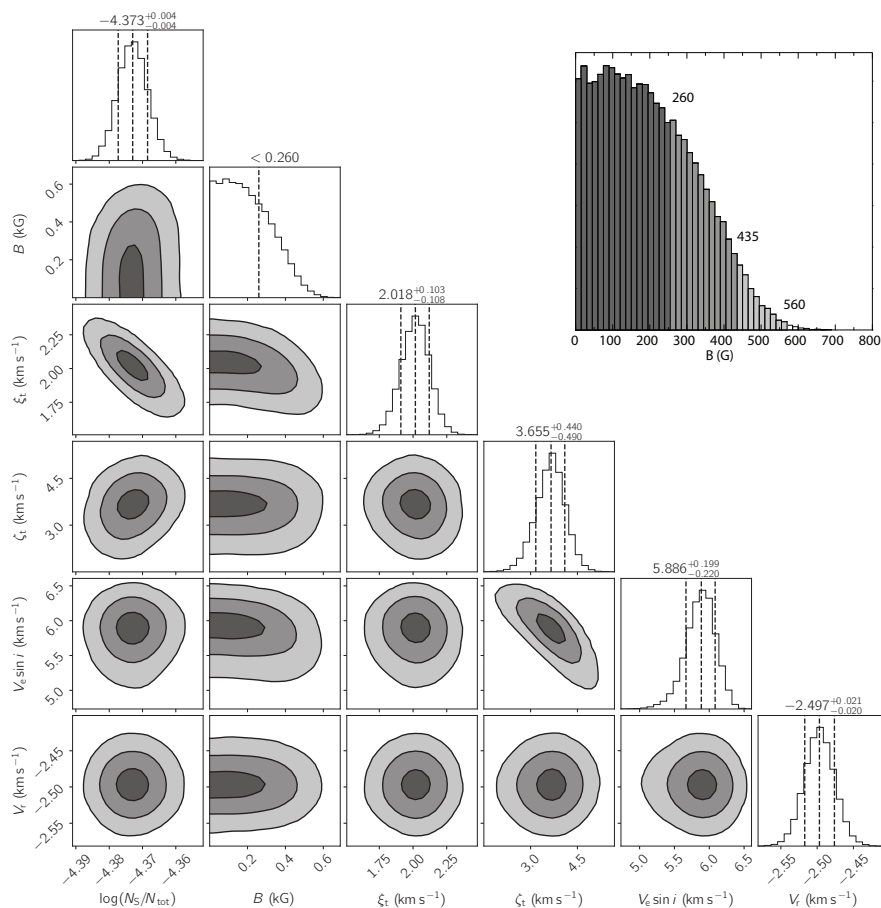


**Fig. 4.** Marginalised posterior distributions of the magnetic field strength and other parameters fitted to the NIR S I triplet. Contours correspond to  $1\sigma$ ,  $2\sigma$ , and  $3\sigma$  confidence levels. The inset in the upper right corner shows posterior distribution of the field strength with the upper limits corresponding to the same set of confidence levels indicated by different shades of grey.

to 2–3 kG and their relative equivalent width is essentially unaffected by PPB for  $B < 4$  kG (Takeda 1991). Thus, in the present study, radiative transfer calculations of the Fe II lines did not include the PPB treatment.

The upper energy levels of the S I triplet studied below differ by 1–2  $\text{cm}^{-1}$ , also making this group of lines potentially susceptible to PPB. Since no previous computation of the PPB splitting exist in the literature for these lines, we have carried out our own assessment using the methods outlined in Landi Degl’Innocenti & Landolfi (2004). This analysis showed that, for the strongest magnetic field considered in Fig. 1a, the PPB effect produces a detectable distortion of the magnetic splitting patterns, leading to slight asymmetries in the doublet-like splitting of the S I 1045.7 and 1045.9 nm lines (Fig. 1b). However, since the subsequent analysis presented in Sect. 4 points to a much weaker, if any, magnetic field in  $\sigma$  Peg, there is no need to incorporate the PPB splitting in our modelling of the S I triplet.

#### 4. Analysis of the near-infrared S I triplet

Based on the magnetic spectrum synthesis calculations described above, we modelled the S I triplet lines in the CRIFES+ spectrum of  $\sigma$  Peg with the help of the Markov chain Monte Carlo (MCMC) technique. For the latter, we employed the IDL implementation by Anfinogentov et al. (2021) with a  $10^4$  step burn-in followed by  $3 \cdot 10^5$  sampling steps. The free parameters included the non-LTE sulphur abundance  $\log N_S/N_{\text{tot}}$ , the microturbulent velocity  $\xi_t$ , the radial-tangential macroturbulent velocity  $\zeta_t$ , the projected rotational velocity  $v_e \sin i$ , the radial velocity shift  $v_r$ , and the magnetic field strength  $B$ . Uniform priors were assumed for all parameters. The treatment of all three velocity fields as

free parameters, without constraints from other lines or previous literature studies, represents a conservative approach likely yielding an increased range of magnetic field strength compatible with observations.

The posterior probability distributions resulting from the MCMC evaluation are presented in Fig. 4. It is evident that for most parameters the calculations have converged on Gaussian-like distributions. There is a noticeable correlation between  $\zeta_t$  and  $v_e \sin i$ , as expected for a narrow-line star. At the same time, the field strength  $B$  shows a one-sided distribution extending all the way to  $B = 0$ . Therefore, according to these results, the observed S I triplet is fully compatible with the null magnetic field. A fit to observations with this model is presented in Fig. 5. The non-magnetic model achieves a near perfect description of the observed profiles. In this case, the standard deviation is 0.36%, which is close to the observational noise. On the other hand, assuming  $B = 2$  kG and allowing all other parameters to vary yields theoretical spectra incompatible with observations (dashed line in Fig. 5, standard deviation 2.86%), even when all other parameters are allowed to vary freely. Repeating the same exercise with theoretical spectra corresponding to  $B = 1$  kG still yields an unsatisfactory fit (standard deviation 0.51%).

The final numerical results of the MCMC calculations are summarised in Table 4. For non-zero parameters we report the median value inferred from the corresponding marginalised probability distribution along with the  $1-\sigma$  (13.6% and 86.4% percentiles) uncertainties. For the magnetic field strength, the  $1-$ ,  $2-$ , and  $3-\sigma$  (68.3, 95.4, and 99.7% confidence levels, respectively) upper limits are given according to the marginalised probability distribution illustrated in the upper right corner of Fig. 4. The  $1-\sigma$  limit is 260 G, which is by far the smallest magnetic

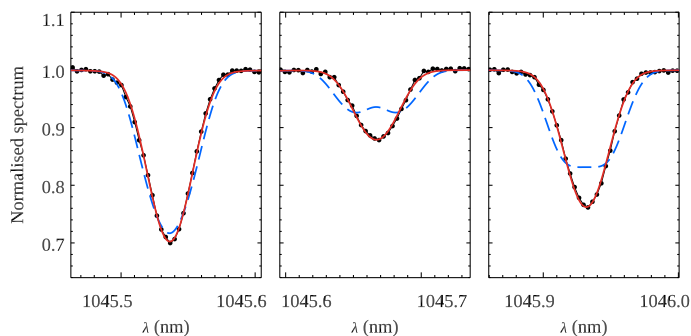


**Fig. 5.** Comparison of the S I lines in the CRIRES<sup>+</sup> observation of *o* Peg (symbols) with the best-fitting non-magnetic model spectrum (solid lines). The dashed lines show an attempt at fitting the data assuming a 2 kG magnetic field.

**Table 4.** Results of MCMC analysis of the S I NIR triplet.

Parameter	Value
$\log N_S/N_{\text{tot}}$	$-4.373 \pm 0.004$
$\xi_t$ (km s <sup>-1</sup> )	$2.02^{+0.10}_{-0.11}$
$\zeta_t$ (km s <sup>-1</sup> )	$3.65^{+0.44}_{-0.49}$
$v_e \sin i$ (km s <sup>-1</sup> )	$5.89^{+0.20}_{-0.22}$
$v_r$ (km s <sup>-1</sup> )	$-2.50 \pm 0.02$
$B_{1\sigma}$ (G)	$\leq 260$
$B_{2\sigma}$ (G)	$\leq 435$
$B_{3\sigma}$ (G)	$\leq 560$

**Notes.** The three bottom rows give upper limits of the magnetic field strength corresponding to  $1\sigma$ ,  $2\sigma$ , and  $3\sigma$  confidence intervals.

field strength limit estimated from a Stokes *I* spectrum of an A-type star. The non-magnetic parameters, in particular  $\xi_t$  and  $v_e \sin i$ , are well within the ranges of determinations by previous studies (e.g. Landstreet et al. 2009; Gray 2014; Adelman et al. 2015). The non-LTE S abundance derived from the NIR triplet,  $[S] = 0.54$ , is also compatible with the measurement of  $[S] = 0.39 \pm 0.10$  from the optical S I and II lines assuming LTE (Adelman et al. 2015).

## 5. Reanalysis of the Fe II 614.7–614.9 nm line pair

The Fe II 614.9 nm line is one of the most commonly used diagnostic lines for detecting Zeeman splitting in the optical spectra of early-type stars. This line has an unusual doublet Zeeman splitting pattern, with two  $\pi$  and two  $\sigma$  components coinciding in wavelength. This simple splitting pattern enables a straightforward detection of  $\geq 2$  kG magnetic fields in mCP stars and robust measurement of the corresponding mean field modulus  $\langle B \rangle$  provided that the stellar projected rotational velocity does not exceed a few km s<sup>-1</sup> (Mathys 1990, 2017; Mathys et al. 1997). Additionally, the Fe II 614.9 nm line shares the upper energy level with the nearby Fe II 614.7 nm transition, which has an almost identical oscillator strength but a very different Zeeman splitting pattern. Similarity of the formation process of these two lines prompted Mathys & Lanz (1990, 1992) to suggest using the relative intensification of this line pair, defined using the equivalent widths of these lines as  $\delta \equiv 2(W_{614.7} - W_{614.9})/(W_{614.7} + W_{614.9})$ , as a proxy of the magnetic field strength for stars showing no discernible splitting of the Fe II 614.9 nm line. Based on the qualitative comparison of  $\delta = 0.052$  measured for *o* Peg with the relative intensification factors observed for several A stars with different magnetic field strengths, Mathys & Lanz (1990) con-

cluded that *o* Peg possess a field of  $\sim 2$  kG. This result agrees with  $B = 2.3$  kG that can be calculated by extrapolating the empirical linear relation between  $\delta$  and  $B$  calibrated by Mathys & Lanz (1992) for the 3–5 kG  $\langle B \rangle$  interval. The magnetic field diagnostic potential of the Fe II 614.7–614.9 nm line pair was further examined by Takeda (1991) using disk-centre polarised radiative transfer calculations and, most recently, by Takeda (2023) assuming an equator-on magnetic field geometry. The former study obtained  $\langle B \rangle \approx 2$ –3 kG while the latter one reported  $\langle B \rangle = 2.3$  kG corresponding to a polar field strength of  $B_d = 3.6$  kG.

These seemingly consistent results notwithstanding, detailed radiative studies of the Fe II line pair by Takeda (1991) and Kochukhov et al. (2013) uncovered several compounding factors and ambiguities in the interpretation of the equivalent width difference of these Fe II lines in terms of the magnetic intensification. Both studies demonstrated that, in the field strength range 0–2 kG, the relation between  $\delta$  and  $B$  is neither linear nor monotonic, rendering the linear relation proposed by Mathys & Lanz (1992) unusable. Moreover, as emphasised by Kochukhov et al. (2013), the  $\delta(B)$  relation depends on the assumption about the local magnetic field orientation, with the radial, horizontal, and turbulent magnetic fields yielding different intensification curves. At the same time, these studies did not consider the impact of the choice of atomic parameters of the Fe II lines and blending by other spectral features on the derived field strength.

Given the apparent major discrepancy between the tight upper limit of  $B \leq 260$  G from our NIR analysis of *o* Peg and repeated claims of 2–3 kG magnetic field from the optical Fe II line pair in this star, we re-examined the latter diagnostic with the spectrum synthesis methodology described in Sect. 3. The line list adopted for our modelling of the Fe II lines is provided in Table 5. It is based largely on information from VALD, with the oscillator strengths of the Fe II lines taken from Raassen & Uylings (1998). This choice yields  $\Delta \log gf = \log gf_{614.7} - \log gf_{614.9} = 0.014$ , implying that the Fe II 614.7 nm line is slightly stronger than the 614.9 nm line in the absence of magnetic field. Our line list also includes the Fe I 614.8 nm line, with the experimental  $\log gf$  value from O’Brian et al. (1991). Although the importance of this blend for interpretation of the equivalent width of the Fe II 614.7 nm line has been mentioned in the literature (Mathys & Lanz 1990; Fossati et al. 2007), it appears to have been discounted in previous detailed radiative transfer studies of this Fe II line pair (Takeda 1991, 2023).

Polarised synthetic spectra were calculated in LTE with Synmast for the same atmospheric parameters as in Sect. 3 assuming a uniform radial magnetic field. Theoretical equivalent widths were obtained with direct integration of line profiles. The same approach was applied to the observed spectra published by Takeda (2023), confirming his measurement of  $\delta = 0.025^2$ . We estimated the uncertainty of this relative equivalent width measurement to be about 0.004 assuming  $S/N=1000$ .

This observed  $\delta$  value is compared with our theoretical  $\delta(B)$  curve in Fig. 6. Taking the uncertainty of the oscillator strength of the Fe I blend into account, our calculations reproduce the observed equivalent width difference of the two Fe II lines without the need to invoke any magnetic field. The observed  $\delta$  is also compatible with our calculations at  $B = 2.2$  kG, illustrating the ambiguity arising from a non-monotonic  $\delta(B)$  relation. We also

<sup>2</sup> This value is significantly smaller than  $\delta = 0.052$  reported for *o* Peg by Mathys & Lanz (1990). We have no explanation for this discrepancy nor why this reduction of the observed  $\delta$  did not result in a corresponding decrease of the field strength inferred by Takeda (2023) compared to Takeda (1991).

**Table 5.** Atomic line data adopted for the analysis of the Fe II 614.7–614.9 nm line pair.

Ion	$\lambda$ (nm)	$\log gf$	$E_{lo}$ (eV)	Lower level		Upper level		$g_{eff}$	$\log \gamma_{rad}$	$\log \gamma_{stark}$	H broadening	
				$J_{lo}$	$g_{lo}$	$J_{up}$	$g_{up}$				$\log \gamma_{vdw}$	$(\sigma_H/a_0^2, \alpha_H)^3$
Fe II	614.77341	$-2.827^1$	3.8887	1.5	1.20	0.5	2.70	0.825	8.50	-6.53		186, 0.269
Fe I	614.78339	$-1.671^2$	4.0758	4.0	1.26	3.0	1.21	1.335	7.55	-6.03	-7.80	
Fe II	614.92459	$-2.841^1$	3.8892	0.5	0.00	0.5	2.70	1.350	8.50	-6.53		186, 0.269

**Notes.** (1) Raassen & Uylings (1998); (2) O’Brian et al. (1991); (3) Barklem et al. (2000); other parameters from VALD, Ryabchikova et al. (2015).

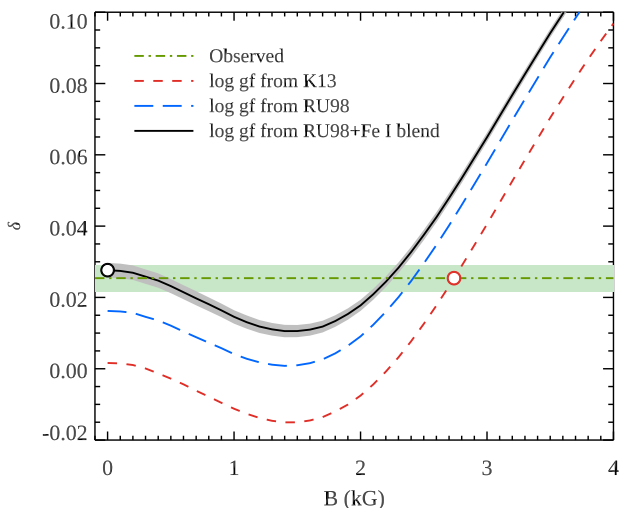


**Fig. 6.** Relative intensification of the Fe II 614.77 and 614.92 nm line pair as a function of magnetic field strength (solid line with the underlying grey curve illustrating  $\pm 1\sigma$  uncertainty arising from the oscillator strength of the Fe I 614.8 nm blend). The horizontal dash-dotted line corresponds to the observed intensification value with the  $\pm 1\sigma$  uncertainty indicated by the green rectangle. The long- and short-dashed lines show theoretical intensification curves for different choices of Fe II oscillator strengths (K13: Kurucz 2013, RU98: Raassen & Uylings 1998) and blending. The two open circles indicate the line parameter-field strength combinations adopted for the synthetic calculations shown in Fig. 7.

show in Fig. 6 another set of calculations in which the Fe I line was ignored. This shifts the intensification curve downwards, requiring  $B = 2.4$  kG to reproduce the observed equivalent width difference. Finally, another choice of the Fe II oscillator strengths favoured by Takeda (2023)<sup>3</sup> yields an even lower  $\delta(B)$  curve, requiring a field strength of 2.7 kG to match the observed  $\delta$ .

Thus, a measurement of the magnetic field in *o* Peg from equivalent widths of the Fe II line pair is generally inconclusive due to ambiguity of the  $\delta(B)$  diagnostic and its dependence on the choice of line parameters. Can we extract useful information from the line profiles themselves? Surprisingly, little attention has been paid to this approach despite high-quality observations and theoretical line profile models being readily available. To this end, Fig. 7 compares the observed profiles published by Takeda (2023) with our Synmast calculations underlying the intensification results presented in Fig. 6. The non-magnetic theoretical spectrum was calculated with the line list from Table 5,

<sup>3</sup> We used  $\log gf_{614.7} = -2.731$  and  $\log gf_{614.9} = -2.732$  according to the semi-empirical calculations by Kurucz (2013). Takeda (2023) adopted  $\log gf_{614.7} = -2.721$  and  $\log gf_{614.9} = -2.724$  corresponding to an older version of Kurucz’s calculations. In both cases, the resulting  $\Delta \log gf$  is smaller than for the oscillator strengths from Raassen & Uylings (1998).

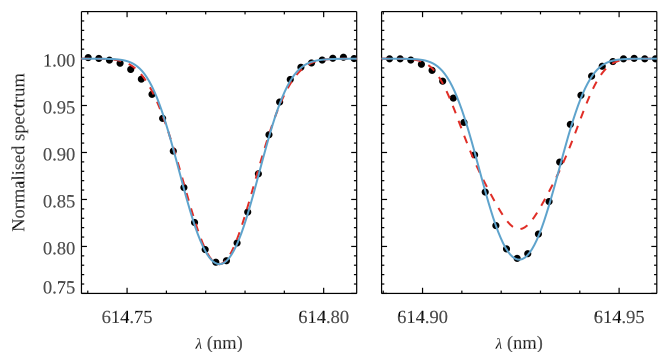


**Fig. 7.** Observed (symbols, Takeda 2023) and calculated (curves) profiles of the Fe II 614.7 and 614.9 nm lines. The solid line shows calculation with the Fe II oscillator strengths from Raassen & Uylings (1998), blending by Fe I 614.8 nm line and no magnetic field. The dashed line corresponds to the synthetic spectrum computed with the oscillator strengths from Kurucz (2013), no Fe I blending, and  $B = 2.7$  kG.

$\xi_i = 2 \text{ km s}^{-1}$ , and other stellar parameters ( $\log N_{Fe}/N_{tot}$ ,  $\zeta_i$ ,  $v_e \sin i$ ) adjusted to fit the Fe II 614.7 nm line. It is evident that this non-magnetic calculation successfully reproduces the Fe II 614.9 nm line without the need to change any line or stellar parameters. Conversely, if we follow Takeda (2023) in adopting the oscillator strengths from Kurucz (2013), ignore the Fe I line and use  $B = 2.7$  kG (required to reproduce the observed  $\delta$  for this choice of parameters, see Fig. 6), no consistent fit for the two lines can be obtained. In this case, the Fe II 614.9 nm line exhibits a reduced central depth and excess broadening compared to Fe II 614.7 nm, both incompatible with observations.

To summarise, our re-analysis of the Fe II 614.7–614.9 nm line pair does not confirm the presence of 2–3 kG magnetic field in *o* Peg. Instead, the observed equivalent widths and profiles of both lines can be successfully reproduced by non-magnetic spectrum synthesis calculations with a plausible choice of transition probabilities and accounting for the contribution of the Fe I 614.8 nm blend. The traditional equivalent width-based analysis of this line pair is ambiguous, as both zero and 2–3 kG field strengths yield the same relative equivalent width difference as derived from observations. However, the strong-field solution is ruled out based on the line profile analysis.

## 6. Constraints on the global magnetic field

There is no evidence of circular polarisation signatures in individual spectral line of *o* Peg despite the high quality of ESPaDOnS observations. In this case, similar to other polarimetric studies of weak magnetic fields in intermediate-mass stars (e.g. Shorlin et al. 2002; Aurière et al. 2010; Makaganiuk et al. 2011), we employed the widely used and thoroughly tested least-squares deconvolution (LSD, Donati et al. 1997; Kochukhov et al. 2010) procedure to derive very high S/N mean Stokes *I*



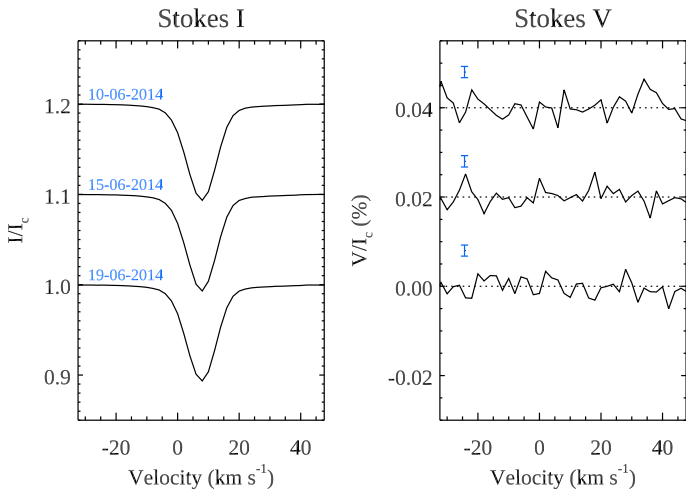


**Fig. 8.** LSD profiles of *o* Peg derived from archival ESPaDOs observations. The two panels show Stokes *I* (left) and *V* (right) profiles offset vertically for display purposes. The UT observing dates are indicated above each Stokes *I* profile.

and *V* profiles. This calculation effectively stacks profiles of all suitable metal lines under the assumption that their profiles are self-similar in velocity space and that the Stokes *V* signal scales with wavelength and effective Landé factor of each line according to the weak-field approximation. The line list for LSD profile calculation was obtained from the VALD database (Ryabchikova et al. 2015), using  $T_{\text{eff}} = 9500$  K,  $\log g = 3.6$  model atmosphere, and elemental abundances from Adelman et al. (2015). Lines deeper than 5% of the continuum were retained and wavelength regions affected by the hydrogen Balmer lines or telluric absorption were excluded. The resulting LSD line mask contained 1483 metal lines, dominated by neutral and singly ionised Fe.

The LSD intensity and polarisation profiles (the latter normalised to the mean wavelength  $\lambda_0 = 500$  nm and effective Landé factor  $z_0 = 1.2$ ) derived from ESPaDOs observations are illustrated in Fig. 8. Application of the LSD procedure resulted in a S/N gain of  $\sim 40$  relative to individual lines, providing a polarimetric precision of  $2.4 \cdot 10^{-5}$ . Despite this, no evidence of Stokes *V* signatures is seen in the Stokes *V* LSD profiles.

The disk-averaged line-of-sight magnetic field component can be characterised by calculating the mean longitudinal magnetic field  $\langle B_z \rangle$  from the Stokes *I* and *V* spectra (e.g. Mathys 1991; Bagnulo et al. 2002). Here we used the prescription by Wade et al. (2000) and Kochukhov et al. (2010) for deriving  $\langle B_z \rangle$  from LSD profiles. The resulting measurements are reported in the last column of Table 2. We achieve no detection of  $\langle B_z \rangle$ , with all three measurements consistent with zero field at the precision of 2.1–2.2 G.

Analysis of LSD profiles derived from high-resolution circular polarisation observations allows us to constrain global magnetic field topologies which produce null  $\langle B_z \rangle$ , for example toroidal field or equator-on dipole. At the same time, one very specific global field configuration – a dipole closely aligned with the stellar rotational axis observed from the stellar equator – will yield no signal in Stokes *V* since spectral contributions from the two stellar hemispheres will cancel out exactly for all rotational phases. This type of global magnetic field geometry, with a polar field of  $B_d = 2\text{--}4$  kG, was advocated by Takeda (2023) to reconcile the absence of polarimetric magnetic detections in *o* Peg with the existence of strong field according to his analysis of intensity spectra. However, our new high-precision polari-

metric measurements suggest that this magnetic configuration is highly improbable. Using the LSD profile modelling procedure described in Metcalfe et al. (2019), we established that it is sufficient for the magnetic obliquity angle  $\beta$  to deviate by  $0.16^\circ$  from  $0^\circ$  or  $180^\circ$  or for the stellar inclination angle  $i$  to deviate by the same amount from  $90^\circ$  for a 3 kG dipolar field to produce Stokes *V* signatures incompatible with observations at  $3\text{-}\sigma$  confidence level. Assuming random orientations of the rotational and magnetic axes, the probability that both  $i$  and  $\beta$  angles fall in the intervals corresponding to no detectable polarimetric signatures is  $< 10^{-8}$ . Thus, the modern high-quality polarimetric data analysed here essentially rule out the possibility that *o* Peg harbours a strong large-scale magnetic field.

## 7. Summary and discussion

In this study, we revisited the question of the presence of a strong magnetic field at the surfaces of metallic-line stars. We focused on the bright Am star *o* Peg, for which the existence of 1–2 kG field covering the entire stellar surface was suggested by studies spanning over three decades (Mathys & Lanz 1990; Lanz & Mathys 1993; Takeda 1991, 1993, 2023). Owing to this series of investigations, *o* Peg is often considered as a prototypical Am star with a strong complex magnetic field. We re-examined archival optical spectra available for *o* Peg and acquired new high-resolution and high S/N near-infrared spectroscopic observations using CRIRES<sup>+</sup> at the ESO VLT. With the help of these NIR observations, we identified the S I triplet at 1046 nm as a particularly useful diagnostic for detecting Zeeman broadening signatures of magnetic field in *o* Peg given its large sulphur overabundance. Modelling these lines with a non-LTE polarised radiative transfer code coupled with a Bayesian inference framework, we concluded that magnetic field of *o* Peg cannot exceed 260 G ( $1\text{-}\sigma$  confidence level). This represents the most sensitive magnetic field upper limit derived from the intensity spectra of an Am star.

Further re-analysis of the Fe II 614.7–614.9 nm line pair, which was previously used to claim magnetic field in *o* Peg, revealed importance of the choice of atomic line parameters and accounting for weak blending. We showed that the observed relative intensification of these lines can be reproduced with either non-magnetic calculations or  $> 2$  kG magnetic field, depending on the adopted line list. However, the profile shape, in particular that of the 614.9 nm Fe II line, is incompatible with the strong-field solution. To summarise, both the optical and NIR spectroscopic data suggests that *o* Peg does not possess a kG-strength magnetic field. If any surface field is present in this star, its strength does not exceed a few hundred G.

The outcome of our re-assessment of the magnetic interpretation of the relative intensification of the Fe II 614.7–614.9 nm lines in *o* Peg is reminiscent of the results of investigations of these lines in the spectra of HgMn stars. For these objects, often considered hotter analogues of Am stars, complex kG-strength magnetic fields claimed from the Fe II line strengths (Hubrig et al. 1999; Hubrig & Castelli 2001) were shown to be incompatible with the lack of Zeeman broadening in high-resolution spectra (Kochukhov et al. 2013). The line intensification analysis was also similarly jeopardised by blending in some HgMn targets (Takada-Hidai & Jugaku 1992). This experience for two distinct classes of CP stars suggests that using the relative intensification of this Fe II line pair to infer magnetic field strength tends to yield spurious results when extrapolated outside the empirically calibrated 3–5 kG field strength interval (Mathys & Lanz 1992). Therefore, some of the recent magnetic field strength estimates

employing the Fe II line ratio (e.g. Holdsworth et al. 2014, 2016; Smalley et al. 2015; Murphy et al. 2020) may not be trustworthy, even when applied to the types of CP stars expected to host strong magnetic fields.

In addition to the analysis of Zeeman broadening and magnetic intensification in Stokes  $I$  spectra, we obtained complementary information on the global magnetic field of  $\alpha$  Peg using unpublished archival optical circular polarisation spectra collected with ESPaDOnS at CFHT. Three observations spread over 10 nights yield null mean longitudinal magnetic field measurements with a typical uncertainty of 2 G. This represents a 10-fold precision improvement compared to the previous  $\langle B_z \rangle$  determinations for  $\alpha$  Peg (Shorlin et al. 2002; Bychkov et al. 2009). Moreover, we reported no evidence of polarisation signatures in S/N  $\approx$  40000 LSD Stokes  $V$  profiles, ruling out the presence of moderately complex non-dipolar global magnetic field topologies.

The non-detection of a magnetic field in polarimetric observations does not necessarily rule out that the star hosts a sizeable surface magnetic field. It can be argued, as was done in previous studies of  $\alpha$  Peg, that the star possesses a dipolar field that happened to be observed nearly equator-on (Takeda 2023) or that the stellar surface field lacks any global component (Mathys & Lanz 1990). However, a high polarimetric accuracy of the Stokes  $V$  LSD profiles derived in our study challenges both of these hypotheses. To remain consistent with the polarimetric non-detections in all three Stokes  $V$  observations, the stellar and dipolar field axes must have a very particular orientation. Namely, both the inclination and magnetic obliquity angles must not deviate by more than  $\approx 0.2^\circ$  from  $90^\circ$  and  $0^\circ$  or  $180^\circ$ , respectively. We showed that the probability to encounter such a magnetic configuration is negligible. On the other hand, the second hypothesis of a highly tangled magnetic field implies the ratio of the total to global field strength of  $\sim 10^3$ , if one adopts the  $\sim 2$  kG total field strength advocated by previous studies of  $\alpha$  Peg. Although the situations of  $\langle B_z \rangle \ll \langle B \rangle$  are not unheard of in stellar magnetometry, this ratio appears to be extremely large for  $\alpha$  Peg compared to  $10^1$ – $10^2$  total to global field amplitudes found in cool active stars with dynamo fields (Kochukhov et al. 2020; Kochukhov 2021). Thus, to accommodate the low  $\langle B_z \rangle$  and high  $\langle B \rangle$  for  $\alpha$  Peg, one would require a qualitatively new type of magnetic field generation process producing a highly structured surface field with a degree of complexity not seen in any other types of stars. However, our results point to a more prosaic explanation: the previous claims of 1–2 kG complex field in  $\alpha$  Peg are erroneous and the actual total field strength does not exceed a few hundred G according to the most sensitive NIR diagnostic. Therefore, this star should be currently considered non-magnetic according to the most sensitive polarimetric and spectroscopic magnetic field detection analyses.

Taking into account results of the present study as well as recent literature, there is no evidence that either globally organised or complex kG-strength magnetic fields exist on the surfaces of Am stars. Instead, Am stars observed with sufficient polarimetric precision appear to possess ultra-weak sub-G fields (Petit et al. 2011; Blazère et al. 2016; Neiner et al. 2017) of unknown geometry. Thus, our work reaffirms the presence of a “magnetic desert” – a conspicuous two orders of magnitude gap in the field strength distribution between the 100–300 G lower field strength bound of mCP stars (Aurière et al. 2007; Kochukhov et al. 2023a) and the sub-G fields of Am stars. The only CP star known to straddle this gap is the marginal Am star  $\gamma$  Gem, which hosts a dipolar field with a polar strength of  $\approx 30$  G (Blazère et al. 2020). It remains to be seen if this object is part of a larger pop-

ulation or represents an extreme example of mCP star, which is in the process of loosing its fossil magnetic field.

*Acknowledgements.* O.K. acknowledges support by the Swedish Research Council (grant agreements no. 2019-03548 and 2023-03667), the Swedish National Space Agency, and the Royal Swedish Academy of Sciences. A.M.A. acknowledges support from the Swedish Research Council (grant agreement no. 2020-03940). H.L.R. acknowledges the support of the DFG priority program SPP 1992 “Exploring the Diversity of Extrasolar Planets (RE 1664/20-1)”. E.N. acknowledges the support by the DFG Research Unit FOR2544 “Blue Planets around Red Stars”. K.P. acknowledges the Swiss National Science Foundation, grant number 217195, for financial support. M.R. acknowledges the support by the DFG priority program SPP 1992 “Exploring the Diversity of Extrasolar Planets” (DFG PR 36 24602/41). D.S. acknowledges financial support from the project PID2021-126365NB-C21 funded by Agencia Estatal de Investigación of the Ministerio de Ciencia e Innovación (MCIN/AEI/10.12039/501100011033). CRIRES<sup>+</sup> is an ESO upgrade project carried out by Thüringer Landessternwarte Tautenburg, Georg-August Universität Göttingen, and Uppsala University. The project is funded by the Federal Ministry of Education and Research (Germany) through Grants 05A11MG3, 05A14MG4, 05A17MG2 and the Wallenberg Foundation.

## References

- Adelman, S. J. 1988, MNRAS, 230, 671  
 Adelman, S. J., Cowley, C. R., Leckrone, D. S., Roby, S. W., & Wahlgren, G. M. 1993, ApJ, 419, 276  
 Adelman, S. J., Gulliver, A. F., & Heaton, R. J. 2015, PASP, 127, 58  
 Albrow, M. D. & Cottrell, P. L. 1996, MNRAS, 278, 337  
 Allen, C. W. 1973, Astrophysical quantities  
 Amarsi, A. M. 2015, MNRAS, 452, 1612  
 Amarsi, A. M., Barklem, P. S., Asplund, M., Collet, R., & Zatsariny, O. 2018a, A&A, 616, A89  
 Amarsi, A. M., Liljegren, S., & Nissen, P. E. 2022, A&A, 668, A68  
 Amarsi, A. M., Nordlander, T., Barklem, P. S., et al. 2018b, A&A, 615, A139  
 Anfinogentov, S. A., Nakariakov, V. M., Pascoe, D. J., & Goddard, C. R. 2021, ApJS, 252, 11  
 Anstee, S. D. & O’Mara, B. J. 1995, MNRAS, 276, 859  
 Aurière, M., Wade, G. A., Lignières, F., et al. 2010, A&A, 523, A40  
 Aurière, M., Wade, G. A., Silvester, J., et al. 2007, A&A, 475, 1053  
 Bagnulo, S., Szeifert, T., Wade, G. A., Landstreet, J. D., & Mathys, G. 2002, A&A, 389, 191  
 Barklem, P. S. 2016, A&A Rev., 24, 9  
 Barklem, P. S. & O’Mara, B. J. 1997, MNRAS, 290, 102  
 Barklem, P. S., O’Mara, B. J., & Ross, J. E. 1998, MNRAS, 296, 1057  
 Barklem, P. S., Piskunov, N., & O’Mara, B. J. 2000, A&AS, 142, 467  
 Belyaev, A. K. & Voronov, Y. V. 2020, ApJ, 893, 59  
 Blazère, A., Petit, P., Lignières, F., et al. 2016, A&A, 586, A97  
 Blazère, A., Petit, P., Neiner, C., et al. 2020, MNRAS, 492, 5794  
 Bychkov, V. D., Bychkova, L. V., & Madej, J. 2009, MNRAS, 394, 1338  
 Caffau, E., Andrievsky, S., Korotin, S., et al. 2016, A&A, 585, A16  
 Cantiello, M. & Braithwaite, J. 2019, ApJ, 883, 106  
 Carlos, M., Amarsi, A. M., & Nissen, P. E. 2024, ApJ, submitted  
 Carrier, F., North, P., Udry, S., & Babel, J. 2002, A&A, 394, 151  
 Cowley, C. R., Ayres, T. R., Castelli, F., et al. 2016, ApJ, 826, 158  
 Debernardi, Y., Mermilliod, J. C., Carquillat, J. M., & Gineset, N. 2000, A&A, 354, 881  
 Donati, J., Catala, C., Landstreet, J. D., & Petit, P. 2006, in Astronomical Society of the Pacific Conference Series, Vol. 358, Astronomical Society of the Pacific Conference Series, ed. R. Casini & B. W. Lites, 362  
 Donati, J.-F. & Landstreet, J. D. 2009, ARA&A, 47, 333  
 Donati, J. F., Semel, M., Carter, B. D., Rees, D. E., & Collier Cameron, A. 1997, MNRAS, 291, 658  
 Dorn, R. J., Bristow, P., Smoker, J. V., et al. 2023, A&A, 671, A24  
 Drake, S. A., Linsky, J. L., & Bookbinder, J. A. 1994, AJ, 108, 2203  
 Dworetsky, M. M. 1993, in Astronomical Society of the Pacific Conference Series, Vol. 44, IAU Colloq. 138: Peculiar versus Normal Phenomena in A-type and Related Stars, ed. M. M. Dworetsky, F. Castelli, & R. Faraggiana, 1  
 Fossati, L., Bagnulo, S., Monier, R., et al. 2007, A&A, 476, 911  
 Ghazaryan, S., Alecian, G., & Hakobyan, A. A. 2018, MNRAS, 480, 2953  
 Gray, D. F. 2014, AJ, 147, 81  
 Grunhut, J. H., Wade, G. A., Neiner, C., et al. 2017, MNRAS, 465, 2432  
 Hahlin, A., Kochukhov, O., Rains, A. D., et al. 2023, A&A, 675, A91  
 Holdsworth, D. L., Kurtz, D. W., Smalley, B., et al. 2016, MNRAS, 462, 876  
 Holdsworth, D. L., Smalley, B., Kurtz, D. W., et al. 2014, MNRAS, 443, 2049  
 Hubrig, S. & Castelli, F. 2001, A&A, 375, 963  
 Hubrig, S., Castelli, F., & Wahlgren, G. M. 1999, A&A, 346, 139  
 Hubrig, S. & Schöller, M. 2021, Magnetic Fields in O, B, and A Stars

- Hui-Bon-Hoa, A. 2000, *A&AS*, 144, 203
- Jermyn, A. S. & Cantiello, M. 2020, *ApJ*, 900, 113
- Kamp, I., Iliev, I. K., Paunzen, E., et al. 2001, *A&A*, 375, 899
- Kaulakys, B. 1991, *Journal of Physics B Atomic Molecular Physics*, 24, L127
- Kochukhov, O. 2007, in *Physics of Magnetic Stars*, ed. I. I. Romanyuk & D. O. Kudryavtsev, 109–118
- Kochukhov, O. 2021, *A&A Rev.*, 29, 1
- Kochukhov, O., Gürsoytrak Mutlay, H., Amarsi, A. M., et al. 2023a, *MNRAS*, 521, 3480
- Kochukhov, O., Hackman, T., & Lehtinen, J. J. 2023b, *A&A*, 680, L17
- Kochukhov, O., Hackman, T., Lehtinen, J. J., & Wehrhahn, A. 2020, *A&A*, 635, A142
- Kochukhov, O. & Lavail, A. 2017, *ApJ*, 835, L4
- Kochukhov, O., Makaganiuk, V., & Piskunov, N. 2010, *A&A*, 524, A5
- Kochukhov, O., Makaganiuk, V., Piskunov, N., et al. 2013, *A&A*, 554, A61
- Korotin, S. A. 2009, *Astronomy Reports*, 53, 651
- Korčáková, D., Sestito, F., Manset, N., et al. 2022, *A&A*, 659, A35
- Kramida, A., Ralchenko, Y., Reader, J., & and NIST ASD Team. 2022, *NIST Atomic Spectra Database (ver. 5.10)*, [Online]. Available: <https://physics.nist.gov/asd>. National Institute of Standards and Technology, Gaithersburg, MD.
- Kurtz, D. W. & Martinez, P. 2000, *Baltic Astronomy*, 9, 253
- Kurucz, R. L. 1995, in *Astronomical Society of the Pacific Conference Series*, Vol. 78, *Astrophysical Applications of Powerful New Databases*, ed. S. J. Adelman & W. L. Wiese, 205
- Kurucz, R. L. 2013, Robert L. Kurucz on-line database of observed and predicted atomic transitions
- Landi Degl'Innocenti, E. & Landolfi, M. 2004, *Astrophysics and Space Science Library*, Vol. 307, *Polarization in Spectral Lines* (Kluwer Academic Publishers)
- Landstreet, J. D. 1992, *A&A Rev.*, 4, 35
- Landstreet, J. D. 2011, *A&A*, 528, A132
- Landstreet, J. D., Kupka, F., Ford, H. A., et al. 2009, *A&A*, 503, 973
- Langhoff, P. W., Sims, J., & Corcoran, C. T. 1974, *Phys. Rev. A*, 10, 829
- Lanz, T. & Mathys, G. 1993, *A&A*, 280, 486
- Lavail, A., Kochukhov, O., & Hussain, G. A. J. 2019, *A&A*, 630, A99
- Lee, H.-W. & Kim, H. I. 2004, *MNRAS*, 347, 802
- Leenaarts, J. & Carlsson, M. 2009, in *Astronomical Society of the Pacific Conference Series*, Vol. 415, *The Second Hinode Science Meeting: Beyond Discovery-Toward Understanding*, ed. B. Lites, M. Cheung, T. Magara, J. Mariska, & K. Reeves, 87
- Lind, K. & Amarsi, A. M. 2024, arXiv e-prints, arXiv:2401.00697
- Makaganiuk, V., Kochukhov, O., Piskunov, N., et al. 2011, *A&A*, 525, A97
- Mathys, G. 1990, *A&A*, 232, 151
- Mathys, G. 1991, *A&AS*, 89, 121
- Mathys, G. 2004a, in *The A-Star Puzzle*, ed. J. Zverko, J. Ziznovsky, S. J. Adelman, & W. W. Weiss, Vol. 224, 225–234
- Mathys, G. 2004b, in *Stellar Rotation*, ed. A. Maeder & P. Eenens, Vol. 215, 270
- Mathys, G. 2009, in *Astronomical Society of the Pacific Conference Series*, Vol. 405, *Solar Polarization 5: In Honor of Jan Stenflo*, ed. S. V. Berdyugina, K. N. Nagendra, & R. Ramelli, 473
- Mathys, G. 2017, *A&A*, 601, A14
- Mathys, G., Hubrig, S., Landstreet, J. D., Lanz, T., & Manfroid, J. 1997, *A&AS*, 123, 353
- Mathys, G. & Lanz, T. 1990, *A&A*, 230, L21
- Mathys, G. & Lanz, T. 1992, *A&A*, 256, 169
- Metcalfe, T. S., Kochukhov, O., Ilyin, I. V., et al. 2019, *ApJ*, 887, L38
- Murphy, S. J., Saio, H., Takada-Hidai, M., et al. 2020, *MNRAS*, 498, 4272
- Neiner, C., Wade, G. A., & Sikora, J. 2017, *MNRAS*, 468, L46
- Nissen, P. E., Akerman, C., Asplund, M., et al. 2007, *A&A*, 469, 319
- O'Brian, T. R., Wickliffe, M. E., Lawler, J. E., Whaling, W., & Brault, J. W. 1991, *Journal of the Optical Society of America B Optical Physics*, 8, 1185
- Petit, P., Lignières, F., Aurière, M., et al. 2011, *A&A*, 532, L13
- Petit, P., Louge, T., Théado, S., et al. 2014, *PASP*, 126, 469
- Piskunov, N. & Valenti, J. A. 2017, *A&A*, 597, A16
- Preston, G. W. 1974, *ARA&A*, 12, 257
- Raassen, A. J. J. & Uylings, P. H. M. 1998, *A&A*, 340, 300
- Rosén, L., Kochukhov, O., Alecian, E., et al. 2018, *A&A*, 613, A60
- Rutten, R. J. 2003, *Radiative Transfer in Stellar Atmospheres*
- Ryabchikova, T., Piskunov, N., Kurucz, R. L., et al. 2015, *Phys. Scr*, 90, 054005
- Savanov, I. S. 1994, *Astrophysics*, 37, 112
- Schöller, M., Hubrig, S., Fossati, L., et al. 2017, *A&A*, 599, A66
- Scholz, G., Lehmann, H., Harmanec, P., Gerth, E., & Hildebrandt, G. 1997, *A&A*, 320, 791
- Scott, P., Grevesse, N., Asplund, M., et al. 2015, *A&A*, 573, A25
- Seaton, M. J., Zeippen, C. J., Tully, J. A., et al. 1992, *Rev. Mexicana Astron. Astrofis.*, 23, 19
- Shorlin, S. L. S., Wade, G. A., Donati, J.-F., et al. 2002, *A&A*, 392, 637
- Shulyak, D., Tsymbal, V., Ryabchikova, T., Stütz, C., & Weiss, W. W. 2004, *A&A*, 428, 993
- Sikora, J., Wade, G. A., Power, J., & Neiner, C. 2019, *MNRAS*, 483, 2300
- Smalley, B., Niemczura, E., Murphy, S. J., et al. 2015, *MNRAS*, 452, 3334
- Smith, K. C. 1996, *Ap&SS*, 237, 77
- Takada-Hidai, M. & Jugaku, J. 1992, *PASP*, 104, 106
- Takada-Hidai, M. & Jugaku, J. 1993, in *Astronomical Society of the Pacific Conference Series*, Vol. 44, *IAU Colloq. 138: Peculiar versus Normal Phenomena in A-type and Related Stars*, ed. M. M. Dworetsky, F. Castelli, & R. Faragiana, 310
- Takeda, Y. 1991, *PASJ*, 43, 823
- Takeda, Y. 1993, *PASJ*, 45, 453
- Takeda, Y. 2023, *Astronomische Nachrichten*, 344, e20220057
- Takeda, Y., Hashimoto, O., Taguchi, H., et al. 2005, *PASJ*, 57, 751
- Takeda, Y., Kang, D.-I., Han, I., et al. 2012, *PASJ*, 64, 38
- van Regemorter, H. 1962, *ApJ*, 136, 906
- Wade, G. A., Bagnulo, S., Kochukhov, O., et al. 2001, *A&A*, 374, 265
- Wade, G. A., Donati, J.-F., Landstreet, J. D., & Shorlin, S. L. S. 2000, *MNRAS*, 313, 851
- Zatsarinny, O. & Bartschat, K. 2006, *Journal of Physics B Atomic Molecular Physics*, 39, 2861
- Zerne, R., Caiyan, L., Berzinsh, U., & Svanberg, S. 1997, *Phys. Scr*, 56, 459
- Zhou, Y., Amarsi, A. M., Aguirre Børsen-Koch, V., et al. 2023, *A&A*, 677, A98